NASA TECHNICAL NOTE

NASA TN D-4053

C.1

NASA TN D-4053

M-1 ENGINE SUBSCALE INJECTOR TESTS

by Herbert E. Scott, Harry E. Bloomer, and Ali H. Mansour

Lewis Research Center
Cleveland, Ohio

NATIONAL AERONAUTICS AND SPACE ADMINISTRATION • WASHINGTON, D. C. • JULY 1967

M-1 ENGINE SUBSCALE INJECTOR TESTS

By Herbert E. Scott, Harry E. Bloomer, and Ali H. Mansour

Lewis Research Center
Cleveland, Ohio

NATIONAL AERONAUTICS AND SPACE ADMINISTRATION

For sale by the Clearinghouse for Federal Scientific and Technical Information
Springfield, Virginia 22151 – CFSTI price $3.00

M-1 ENGINE SUBSCALE INJECTOR TESTS

by Herbert E. Scott, Harry E. Bloomer, and Ali H. Mansour

Lewis Research Center

SUMMARY

Subscale tests were conducted to assess the performance-stability tradeoff of several M-1 engine injector-element configurations. The tests were conducted at 15 000 pounds thrust with a 5.39-inch-diameter chamber. The chamber pressure (1040 psia nominal at the injector face), flow per element, element spacing, contraction ratio (1.7:1), and chamber length (29 in.) of the M-1 engine were duplicated. Tests at reduced chamber pressure and with 44-inch chambers were also run.

At design conditions, the fine injector had 99-percent characteristic-exhaust-velocity efficiency, while the coarse-injector efficiency was slightly lower. Coarse-injector efficiency dropped off as hydrogen-injector temperature was decreased, while fine-injector performance was unaffected by temperature. Coarse-injector low-temperature efficiency was increased by both oxygen-tube recess and longer chambers. Oxygen-tube recess increased the hydrogen-injection differential pressure drop. No instability was encountered at nominal engine-design conditions. The coarse injector chugged at chamber pressures below 850 psia; however, it did not induce high-frequency combustion instability under any test conditions. The fine injector experienced no chugging, even for chamber pressures of less than one-half of nominal, but it did exhibit a very low-amplitude longitudinal mode of combustion instability below 70° R when this injector was used with the 44-inch chamber.

INTRODUCTION

Concurrent with the rapidly expanding space program has come the need to lift larger and larger payloads. One of the more obvious means of lifting larger payloads is to increase the size of the booster stages and associated rocket engines. The M-1 engine, at 1 500 000 pounds thrust, is by far the largest hydrogen-oxygen engine ever built. However, several problem areas arise as engine size is increased. One of the most elusive problems is high-frequency combustion instability. Coarsening the injector by decreasing the number of injector elements, and thereby increasing thrust per

element, was shown in reference 1 to increase stability characteristics, although a penalty of lower performance was incurred at very low hydrogen temperatures. A correlation presented in reference 2 also indicates that stability increases as element size increases. As a result of this apparent performance-stability tradeoff, subscale experiments on the M-1 rocket-engine injector-element configurations were necessary.

Accordingly, subscale tests were conducted at the Lewis Research Center to assess the performance and the chugging stability characteristics of the several M-1 engine injector-element configurations. Some indications of the high-frequency characteristics were also obtained. Effects on performance and stability of number of injector elements, oxidizer-tube recess, oxidizer-tube taper ream, film cooling, and chamber length were investigated.

The subscale tests were conducted at the reduced thrust level of approximately 15 000 pounds, which was achieved by reduction of chamber diameter from 42.0 to 5.39 inches. The chamber pressure (nominally 1040 psia at the injector face), flow per element, element spacing, contraction ratio (1.7:1), and chamber length (29 in. from injector face to nozzle throat) of the M-1 engine were duplicated. Additional tests at lower chamber pressures were made to assess chugging instability characteristics. Also, combustion chambers 44 inches long were run to assess high-frequency combustion instability. Even though tangential modes were not expected, it was hoped that the behavior of any longitudinal mode might be indicative of stability characteristics of the elements in a large chamber.

APPARATUS

Test Facility

The rocket-engine test facility of the Lewis Research Center is a remotely operated 50 000-pound-thrust sea-level stand. A pressurized propellant system delivered the propellants, liquid oxygen and a mixture of liquid and gaseous hydrogen, to the engine from storage tanks. Oxygen was delivered to the engine from a 55-cubic-foot liquid-nitrogen-jacketed tank through a similarly jacketed line. Liquid hydrogen flowed to the hydrogen-mixing station from a 175-cubic-foot evacuated-perlite-jacketed Dewar through a vacuum-jacketed line. Gaseous hydrogen flowed to the hydrogen-mixing station from a 2200-pound-per-square-inch, 120 000-standard-cubic-foot, gaseous-hydrogen bottle farm through a high-pressure line. Mixing of the liquid and gaseous hydrogen was accomplished by swirling the liquid hydrogen into the gaseous-hydrogen stream. The engine was ignited with gaseous fluorine (supplied through the oxidizer dome) prior to oxygen flow initiation. Sketches of the facility and a more detailed description may be found in reference 3.

Engine

The basic subscale engine was comprised of a concentric-tube injector, a cylindrical heat-sink thrust chamber, and a convergent-divergent heat-sink nozzle as illustrated in figure 1 (fine-element injector shown). Faceplate views of a coarse injector (thrust per element, 1267 lb) with 19 elements and a fine injector (thrust per element, 462 lb) with 51 elements are shown in figures 2 and 3, respectively. The faceplate in each case was fabricated from 0.30-inch-thick 347-stainless-steel sintered wire cloth having a permeability of 300 standard cubic feet per minute of air at a differential pressure of 20 pounds per square inch. Figure 2 shows the forty-eight 0.070-inch-diameter film-cooling holes drilled through the Rigimesh face around the injector periphery. These holes were used for only one set of test data.

The injector elements, furnished by the M-1 engine manufacturer, were full-scale engine production elements. Basic design of the elements was taken from the J-2 engine development work. Modifications, such as taper reaming of the oxygen tubes and decreasing hydrogen-to-oxygen injection area ratio (hence increasing injection velocity ratio), were made based on previous Lewis Research Center work reported in reference 3. The coarse-element injector was selected because calculations showed it to be the most stable injector that would operate at a tolerable efficiency. The fine-element injector was selected for optimum performance without undue fabrication problems. It was expected to be less stable though, hopefully, not enough so that it would be necessary to use the potentially lower-performing, coarse backup injector. The fine-element configurations had a design-point hydrogen-to-oxygen velocity ratio of about 18 at the design-point hydrogen-injector temperature of 140° R, while the coarse elements had a ratio of about 6.

A cross-sectional view of the coarse injector-element configurations is shown in figure 4. Both configurations, 1a and 1b, have a 30° swirler and were identical with the exception that the oxygen tube is recessed 0.2 inch in configuration 1b.

Cross-sectional views of the four fine-injector-element configurations are shown in figure 5 where their differences may be noted. Just a few tests had been made with configuration 2a when it was decided that the oxygen-tube entrance should be modified to incorporate a greater restriction as a deterent to chugging instability. A slight enlargement in the oxygen-tube-exit area was also incorporated in the second fine-element configuration 2b. Configuration 2c differed from 2b only in the oxygen-tube-exit outer diameter, which was slightly smaller in configuration 2c; this condition resulted in a slightly larger hydrogen-tube-exit area. The oxygen tube of configuration 2c was taper reamed at a 7° angle to produce configuration 2d shown in figure 5(c). Taper reaming of the assembled injector resulted in slight flaring of the tube exit, which yielded a slightly larger outer diameter and decreased the hydrogen area by about 10 percent.

This change caused an increased hydrogen-to-oxygen velocity ratio, which was reported in reference 3 to be advantageous from performance and stability standpoints.

A heavy-wall, carbon-steel thrust chamber with a coating of 0.018 inch of zirconia on top of a 0.012-inch coating of nickel chromium alloy was used. The nozzle converged from the chamber diameter of 5.39 inches (42.0 in. on M-1 engine) to a throat diameter of 4.15 inches which gave a contraction ratio of 1.7:1 (same as for the M-1 engine). The short divergent section had an expansion ratio of 1.7:1 (40:1 on M-1 engine) since the tests were conducted in a sea-level rocket facility and since combustion performance was unaffected by the nozzle geometry. As indicated in the INTRODUCTION, most of the testing was done with a 29-inch chamber, though a 44-inch chamber was used for a number of tests.

Instrumentation

Instrumentation used in the investigation is shown in figure 6. Signals from the transducers were transmitted to the control room and to the automatic digital data recorder. Raw data were converted to rocket performance parameters by means of the calculation methods detailed in appendix A.

Piezoelectric-type, quartz, water-cooled, flush-mounted pressure transducers were used at three locations on the thrust chamber, as shown in figure 6. These transducers determined the character and phase relation of the pressure field, hence facilitating mode identification should screech occur. Response characteristics of the high-frequency transducers as installed were flat to within 10 percent to a frequency of 6000 hertz and had a nominal resonant frequency of 130 000 hertz. Signals from the high-frequency transducers were recorded in analog form on magnetic tape and on oscillograph paper for visual study immediately after each test.

Oxygen-propellant weight flow was determined with a vane-type flowmeter which was calibrated with water by means of a static weighing system. The correction from water calibration to cryogenic calibration, which accounted for the dimensional change of the instrument with temperature, was obtained from the flowmeter manufacturer. Liquid-hydrogen weight flow was measured with a venturi, and the gaseous-hydrogen weight flow was measured with an orifice plate. The strain-gage-type pressure transducers were calibrated by a commercial standard. Temperatures were measured by platinum resistance-type sensors described in reference 2. Immediately prior to data acquisition the pressure and temperature systems were calibrated by an electrical two-step calibration system that used resistances in an electrical circuit to simulate a given pressure. The estimated maximum error in injector performance caused by measurement errors was determined to be approximately ±2 percent.

Originally, water-cooled thrust chambers were planned for the program which would have enabled better accuracy because of the longer run times. However, these chambers were not available because of the scheduling of the program, and heat-sink chambers were utilized. Both the short run times and the nozzle-throat erosion which occurred on some of the runs contributed to data scatter.

PROCEDURE

The oscillograph record of a typical test is shown in figure 7. An electrical timer was used to properly sequence all operations during each run. A liquid-hydrogen precool was used to condition the hydrogen feed system. Hydrogen-injector temperature was controlled by varying the ratio of liquid to gaseous hydrogen.

For those runs when screech was encountered, the experimental data were read at the point where a high-frequency pressure transducer indicated screech had started. Screech was considered to start when a periodic waveform with an amplitude greater than a noise level of approximately 2 percent of chamber pressure was observed on the oscillograph trace.

Runs were kept short (usually less than 3/4 sec) to minimize erosion. The engine was inspected after each series of runs and any erosion was noted.

RESULTS AND DISCUSSION

The results, and accompanying discussions, will be presented in three sections -- performance, injection characteristics, and stability characteristics. The experimental data are presented in table I. Nominal operating conditions of the M-1 thrust chamber are a chamber pressure of 1040 psia at an oxidant-fuel ratio (O/F) of 5.5 and a hydrogen-injector temperature of 140° R.

Performance

Performance will be expressed in terms of characteristic exhaust velocity efficiency (C* efficiency) expressed as a percentage. As detailed in appendix A, this efficiency is defined as the ratio of experimental characteristic exhaust velocity to theoretical characteristic exhaust velocity with an assumed equilibrium composition during expansion (ref. 4). Performance plots will contain only data points with an O/F of 5.5 ± 1.0.

Performance of the coarse-injector configurations as a function of hydrogen-

injector temperature is presented in figure 8. There is no appreciable C* efficiency difference between configuration 1a with 17-percent film cooling and the same configuration without film cooling. This result could be due to the large length to diameter ratio of the chamber, and the same effect would not be expected at the full-scale thrust-chamber diameter of 42 inches. Configuration 1a does exhibit an appreciable drop in efficiency as hydrogen-injector temperature is decreased below 140° R. The 0.2-inch recess of the oxygen tube in configuration 1b appears to slightly increase the efficiency at 140° R from 97.5 to almost 99 percent. Recessing definitely decreased the performance dropoff with decreasing hydrogen-injector temperature since the efficiency of configuration 1b dropped only about 1 percentage point at a temperature of 95° R compared to 3 percentage points for configuration 1a. Configuration 1b had approximately 8 points higher efficiency at 68° R than had configuration 1a. Increasing chamber length from 29 to 44 inches with configuration 1b further increased efficiency at low temperatures by 2 percentage points.

The effect of hydrogen-injector temperature on the efficiency of the fine injector is shown in figure 9. The efficiency is approximately 99 percent for all four fine-element configurations. However, the efficiency of the 29-inch chamber configurations may not hold up at the lower temperatures as there are no data points below 100° R for these configurations.

In summary, figures 8 and 9 indicate that the fine injector is slightly superior in performance to the coarse injector. This advantage is only a fraction of a percent at 140° R, but it is greater at lower hydrogen temperatures.

Reference 3 has indicated that in order to keep the performance high at low hydrogen-injector temperatures, the injection velocity ratio should be high. The difference in efficiency, then, may be attributable to the fact that the coarse-injector configurations had much lower velocity ratios than had the fine-pattern configurations. Element configuration 2d was chosen for the full-scale injector tests. Variations in operating parameters were then made in these small-scale tests in order to obtain more performance information for this element.

The effect of oxidant-fuel ratio on C* efficiency of configuration 2d is presented in figure 10 for a nominal 140° R hydrogen-injector temperature and 1040-psia chamber pressure. Two data points at lower chamber pressures are used to extrapolate the curve to mixture ratio extremes. The line drawn through the data points indicates a slight dropoff in efficiency at high mixture ratios. This dropoff from a mixture ratio of 4.5 to 6.5 amounts to about 1 percentage point in efficiency.

Presented in figure 11 is the effect of chamber pressure on C* efficiency of configuration 2d at a nominal hydrogen-injector temperature of 140° R. The line drawn through the data points shows a drop in efficiency from 99 percent at a chamber pressure of 900 psia to 95 percent at a pressure of 440 psia.

Injection Characteristics

The relation between propellant flows and injection differential pressures are presented in figures 12 and 13. Flow rates are divided by the number of injector elements; this makes the results comparable to the single-element tests reported in reference 5.

In figure 12, the oxygen flow varies with the square of the injection differential pressure as expected for an incompressible fluid. Table II shows a comparison between the oxygen-injection differential pressure values at design flow rates presented in reference 5 and those of this report. The oxygen-injection differential pressure of configuration 1b (with 0.2-in. recess) is equal to that of configuration 18c from reference 5 (with 0.3-in. recess). However, the results of reference 5 show an element-recess effect, while data presented in this report do not show such an effect. The slight variation in oxygen-exit diameter should have negligible effect.

The oxygen-injection differential pressure of the tapered fine element of configuration 2d is slightly lower than that of the similar element of reference 5 (configuration 21g). The effect of oxygen-orifice size on differential pressure between configuration 2a and configurations 2b and 2c should be noted. The differential pressure relation is not a square root function, however, because of the higher entrance orifice losses of configuration 2a. Taper reaming had no effect on the differential pressure. Again, the slight variation in oxygen-exit diameter should have negligible effect.

Hydrogen flow per element is presented as a function of the hydrogen-injection normalization factor (square root of density times differential pressure) in figure 13. The configuration 1a with film-cooling line (on the right) will coincide with the line for configuration 1a without film cooling if the flow is adjusted to reflect only that portion that passed through the elements. A slight increase in the normalization factor is caused by the 0.2-inch oxidant-tube recess. Apparently this increase is due to interaction with oxygen in the cup formed by the recess.

For the fine-element configurations, a difference in normalization factor between the line of configurations 2a and 2b and that of configuration 2c should be noted. This difference is the result of the larger oxygen-tube outer diameter of configuration 2c. Configuration 2d exhibits an even higher normalization factor. Two conditions which may contribute to this difference in normalization factors are the slight flaring of the oxygen tubes during taper reaming and increased interaction with the oxygen stream.

Table III shows the excellent agreement between configuration 1b and configuration 18 (from ref. 5) and similarly between configuration 2d and configuration 21g (ref. 5). Configuration 18c (ref. 5), which has a 0.1-inch-deeper recess than configuration 1b, exhibits a much higher pressure drop; thus, the oxygen interaction hypothesis mentioned previously is substantiated.

Stability Characteristics

No instability was encountered with any injector configuration at nominal engine-design conditions. Low-frequency combustion instability, or chugging, occurred during many start transients and throughout five coarse-injector runs at chamber pressures below 850 psia. The fine elements were designed to have a good margin from chugging instability at the design point. Even at chamber pressures as low as 400 psia, no chugging was observed. High-frequency combustion instability, or screech, was present during two runs with the fine injector in a 44-inch-long chamber at off-design conditions.

A typical oscillograph trace of chugging is presented in figure 14. The high-frequency transducer recorded a 165-psi peak-to-peak amplitude at a frequency of 180 hertz at the end of the run. A tabulation of the five chugging runs and the pertinent parameters is presented in table IV.

The low-frequency phenomena are usually linked to feed-system pressure drops, flow relations, and dead time criteria. A recent "double dead time" analysis is reported in reference 6, which advances a stability model in which each propellant undergoes a discrete dead time. The model is simplified in that neither the effects of the feed system nor the pressure and velocity sensitivities of the dead times were considered. These data points can be fitted to this stability model. However, not enough data points are available to clearly define stability over a range of chamber pressures and propellant-injection pressure drops; additional points would be required to provide a complete confirmation of the stability model.

During the 66 rocket runs which comprise this investigation, high-frequency instability was observed only two times. Both runs were with the 44-inch-long combustion chamber and fine-element-injector configuration 2c. Furthermore, screech occurred only when the chamber pressure and the hydrogen-injector temperature were reduced simultaneously below rated conditions. These two runs, with their screech parameters, are listed in table V.

The power spectral densities of screech occurrences are presented in figure 15. In this figure, the screech amplitude is less than 5 percent of chamber pressure for both runs. Only longitudinal modes were encountered, as was anticipated with this long, small-diameter chamber; this finding was based on work reported in reference 7 and on work done at Lewis Research Center. Transverse instabilities were not expected because of the relatively small-diameter combustion chamber and the relatively coarse-pattern injectors which would result in distributed combustion which tends to promote stability. It has been hoped that any longitudinal instability might yield some values of the sensitive time lag of these elements and that this value could be applied to the full-scale combustor. Because the instability occurred at low chamber pressures, and in

both first and second longitudinal modes, the estimated sensitive time lags are not considered applicable to the full-scale combustor.

CONCLUDING REMARKS

The application of these subscale results of this investigation to the full-scale chamber tests of the M-1 can be interpreted as follows:

(1) The fine-injector-element performance leaves little or no room for improvement.

(2) The coarse-injector elements could be employed with very little performance penalty.

(3) The high injection differential pressures and the high design velocity ratios of the fine elements are deterrents to chugging and high-frequency instability problems, respectively.

SUMMARY OF RESULTS

Subscale tests conducted to assess the performance-stability tradeoff of several M-1 engine injector-element configurations produced the following results:

1. Fine-injector performance was 99 percent of equilibrium theoretical characteristic exhaust velocity.

2. At nominal conditions, coarse-injector performance was slightly lower than that of the fine injector; this difference in performance was probably due to the lower design velocity ratio. Performance dropped off as hydrogen-injection temperature was decreased below 140° R. Both oxygen-tube recess and longer chambers increased the efficiency at the lower temperatures.

3. Performance of the tapered fine injector decreased from 99 to 96 percent as chamber pressure was decreased from nominal to 0.4 of nominal, but combustion remained stable with no chugging.

4. Oxygen-tube recess increased the hydrogen-injection differential pressure drop.

5. No instability was encountered at nominal engine-design conditions. Chugging was encountered with the coarse injector when chamber pressure was less than 850 psia. Low-amplitude screech was encountered with the fine injector at temperatures below 90° R and at chamber pressures well below nominal.

Lewis Research Center,
National Aeronautics and Space Administration,
Cleveland, Ohio, February 21, 1967,
128-31-06-05-22.

APPENDIX A

CHARACTERISTIC EXHAUST VELOCITY EFFICIENCY

Characteristic exhaust velocity efficiency is calculated in the following manner (symbols are defined in appendix B):

$$\eta_{C^*} = \frac{C^*_{exp}}{C^*_{th}}$$

where C^*_{th} is from reference 4, and

$$C^*_{exp} = \frac{P_c A_t g}{\dot{W}}$$

$$P_c = \frac{P_{inj}}{MPL}$$

$$MPL = \frac{P_1}{P_c} + \frac{I_1 g - V_{avg}}{C^*_{th} \epsilon}$$

$$V_{avg} = \frac{V_{H_2} \dot{W}_{H_2} + V_{O_2} \dot{W}_{O_2}}{\dot{W}}$$

APPENDIX B

SYMBOLS

A_{ch} area of chamber, $in.^2$

A_t area of throat, $in.^2$

C^*_{exp} experimental characteristic exhaust velocity, ft/sec

C^*_{th} theoretical characteristic exhaust velocity, ft/sec (ref. 4)

f frequency, Hz

g gravitational conversion factor, (lb mass - ft)/(lb force - sec^2)

I_1 theoretical specific impulse at nozzle inlet, (lb force - sec)/lb mass (ref. 4)

MPL momentum pressure loss

ΔP hydrogen-injection differential pressure, psi

P_c total pressure in nozzle, psia

P_{inj} chamber pressure at injector face, psia

P_1 static pressure at nozzle inlet, psia

V_{avg} average injection velocity, ft/sec

V_{H_2} hydrogen-injection velocity, ft/sec

V_{O_2} oxygen-injection velocity, ft/sec

$\dot{W}$ propellant weight flow, lb mass/sec

$\dot{W}_{H_2}$ hydrogen weight flow, lb mass/sec

$\dot{W}_{O_2}$ oxygen weight flow, lb mass/sec

ϵ contraction ratio, A_{ch}/A_t

η_{C^*} characteristic exhaust velocity efficiency, percent

ρ hydrogen density, lb mass/ft^3

REFERENCES

1. Hannum, Ned P.; and Conrad, E. William: Performance and Screech Characteristics of a Series of 2500-Pound-Thrust-Per-Element Injectors for a Liquid-Oxygen - Hydrogen Rocket Engine. NASA TM X-1253, 1966.

2. Reardon, Frederick H.: Combustion Stability Characteristics of Liquid Oxygen/Liquid Hydrogen at High Chamber Pressures. Paper No. 65-612, AIAA, June 1965.

3. Wanhainen, John P.; Parish, Harold C.; and Conrad, E. William: Effect of Propellant Injection Velocity on Screech in 20,000-Pound Hydrogen-Oxygen Rocket Engine. NASA TN D-3373, 1966.

4. Sievers, Gilbert K.; Tomazic, William A.; and Kinney, George R.: Theoretical Performance of Hydrogen-Oxygen Rocket Thrust Chambers. NASA TR R-111, 1961.

5. Kovach, R.: M-1 Uni-element Program Engineering Data Compilation. Rep. No. AGC 8800-57, Aerojet-General Corporation, Feb. 15, 1966.

6. Wenzel, Leon M.; and Szuch, John R.: Analysis of Chugging in Liquid-Bipropellant Rocket Engines Using Propellants With Different Vaporization Rates. NASA TN D-3080, 1965.

7. Crocco, Luigi; Grey, Jerry; and Harrje, David T.: Theory of Liquid Propellant Rocket Combustion Instability and its Experimental Verification. ARS J., vol. 30, no. 2, Feb. 1960, pp. 159-168.

TABLE I. - EXPERIMENTAL DATA FROM SUBSCALE INJECTOR TESTS

Test	Run duration, sec	Element configuration	Film cooling	Chamber length, in.	Oxygen-injector area, $in.^2$	Hydrogen-injector area, $in.^2$	Chamber pressure at injector face, P_{inj}, psia	Oxidant-fuel ratio, O/F	Hydrogen-injector temperature, ^oR	Characteristic-exhaust-velocity efficiency, η_{C^*}, percent	Oxygen-injection differential pressure, psi	Hydrogen-injection differential pressure, ΔP, psi	Oxygen weight flow, $\dot{W}_{O_2}$, lb mass/sec	Hydrogen weight flow, $\dot{W}_{H_2}$, lb mass/sec
43	1.13	1a	Yes	29	0.749	1.093	1011	4.84	191	97.7	166	255	45.15	9.33
44A	1.73	↓	↓	↓	↓	↓	1007	5.17	151	----	183	164	47.32	9.16
44B	1.73	↓	↓	↓	↓	↓	1000	4.93	77	90.2	187	70	48.37	9.81
49	.51	↓	No	↓	↓	.908	1044	4.74	200	97.3	208	382	46.93	9.90
50	.65	↓	↓	↓	↓	↓	1046	5.21	105	95.8	191	160	48.75	9.36
51	.67	↓	↓	↓	↓	↓	1058	5.59	142	97.7	190	224	49.62	8.87
52	.60	↓	↓	↓	↓	↓	1036	5.36	67	86.5	213	113	54.00	10.08
53	.64	↓	↓	↓	↓	↓	995	7.68	128	93.0	247	134	55.60	7.24
64	.74	1b	↓	↓	↓	↓	1036	5.91	170	97.8	195	276	50.55	8.55
65	.66	↓	↓	↓	↓	↓	1030	5.64	68	95.6	202	102	50.46	8.94
66	.59	↓	↓	↓	↓	↓	1048	5.73	126	100.0	187	193	49.37	8.62
67	.65	↓	↓	↓	↓	↓	1046	6.13	140	98.9	210	202	51.01	8.32
68	.66	↓	↓	↓	↓	↓	1046	5.33	137	98.6	195	234	48.82	9.16
97	.87	↓	↓	↓	↓	↓	303	4.45	250	79.4	---	62	16.05	3.61
98	1.50	↓	↓	↓	↓	↓	286	4.97	230	87.1	17	65	14.31	2.88
99	1.50	↓	↓	↓	↓	↓	258	4.43	97	81.4	13	21	13.42	3.03
100	1.54	↓	↓	↓	↓	↓	319	2.32	65	90.1	--	66	12.82	5.53
101	.97	↓	↓	↓	↓	↓	654	4.49	133	99.6	60	175	28.17	6.27
102	1.02	↓	↓	↓	↓	↓	660	3.76	68	95.1	--	80	28.22	7.50
103	1.05	↓	↓	↓	↓	↓	637	2.47	63	96.8	--	132	24.25	9.81
104	.63	↓	↓	44	↓	↓	---	6.42	126	----	--	193	52.66	8.20
105	.61	↓	↓	↓	↓	↓	1066	5.24	65	98.2	168	108	48.70	9.29
106	.64	↓	↓	↓	↓	↓	1060	5.17	61	95.9	161	115	49.40	9.55
107	.64	↓	↓	↓	↓	↓	1065	5.67	63	96.0	171	103	50.80	8.97
108	.62	↓	↓	↓	↓	↓	1052	6.10	93	98.8	161	145	50.20	8.23

126	.68	1b	No	29	0.749	0.908	866	5.46	196	98.7	186	317	39.77	7.28
127	.64						860	4.59	104	97.9	124	174	37.78	8.23
128	.65						873	4.82	135	99.3	116	232	38.35	7.95
129	.69						837	4.17	98	98.8	109	165	35.45	8.50
130	.67						762	7.28	143	99.8	120	140	38.57	5.30
131	.64						814	5.07	121	99.6	110	185	36.35	7.17
54	.66	2a			1.298	0.886	1026	5.07	137	97.8	181	134	46.54	9.18
55	.60						1041	4.17	70	99.2	220	80	43.86	10.52
56	.72						1076	5.12	105	99.5	258	100	48.00	9.37
57	.67						1042	4.92	122	100.5	235	132	45.50	9.25
60	.65	2b		44	1.594		1105	5.14	165	97.5	365	173	50.64	9.86
61	.67						1048	4.81	69	97.4	440	80	46.85	9.75
62	.59						1068	5.30	72	98.6	390	58	48.54	9.15
211	.87	2c		29		1.086	554	5.07	65	100.1	85	34	24.19	4.77
213	.85			44			1013	4.68	140	99.0	264	194	43.64	9.32
214	.80						1028	4.31	60	97.7	268	86	43.60	10.11
215	.88						1042	4.79	60	100.3	296	75	44.61	9.31
216	.86						1007	5.18	66	100.8	283	70	43.69	8.43
217	.85						554	7.47	90	84.5	166	28	33.47	4.48
218	.78						861	5.93	67	95.8	254	48	41.18	6.95
219	.87						767	5.73	68	93.9	205	48	37.08	6.47
502	.73	2d		29	2.503	.969	1018	5.62	184	99.3	302	266	46.10	8.20
503	.74						1038	5.03	133	99.9	299	203	45.06	8.95
504	.67						1052	4.35	107	96.6	294	188	45.14	10.37
505	.69						994	5.66	76	----	508	262	49.05	8.66
506	.72						1085	5.49	132	----	401	195	52.36	9.54
507	.71						1037	6.20	165	----	432	221	54.22	8.74
512	.67						1087	6.44	131	99.0	384	156	52.24	8.11
513	.75						1074	5.87	132	97.5	377	176	50.75	8.64
514	.70						958	6.09	126	----	337	149	47.50	7.80
516	.75						897	6.95	156	97.7	292	149	45.05	6.48
517	.72						809	4.30	137	100.4	182	188	33.77	7.86
518	.63						874	5.79	142	99.1	242	153	40.52	7.00
519	.73						697	5.03	135	96.4	153	136	31.66	6.30
520	.73						434	5.34	166	95.7	65	86	20.50	3.84
521	.69						547	5.56	167	97.1	107	119	25.68	4.62

TABLE II. - OXYGEN-INJECTION DIFFERENTIAL PRESSURES

Element configuration	Oxygen-tube recess, in.	Oxygen-injection differential pressure, psi	Oxygen weight flow per element lb mass/sec	Oxygen-tube-exit diameter, in.	Comments
Coarse:					
1a	0	200	2.620	0.224	Swirler
[a]18	.15	172	↓	.220	↓
1b	.20	200		.224	
[a]18c	.30	199		.220	
Fine:					
2a	0.20	235	0.890	0.180	Straight, 0.118-in. orifice
2b and 2c	↓	300	↓	.200	Straight, 0.100-in. orifice
2d		300		.250	Tapered, 0.100-in. orifice
[a]21g		336		.257	Tapered, 0.100-in. orifice

[a]Data from ref. 5.

TABLE III. - HYDROGEN-INJECTION DIFFERENTIAL PRESSURE

Element configuration	Oxygen-tube recess, in.	Hydrogen-injection normalization factor, $\sqrt{\rho \Delta P}$	Hydrogen weight flow per element, lb mass/sec	Comments
Coarse:				
1a	0	17.5	0.426	Straight
[a]18	.15	19.0	↓	↓
1b	.20	18.4		
[a]18c	.30	29.3		
Fine:				
2a and 2b	0.20	12.2	0.147	Straight
2c	↓	14.5	↓	Straight
2d		15.5		Tapered
[a]21g		17.2		Tapered

[a]Data from ref. 5.

TABLE IV. - COARSE-INJECTOR CHUGGING TABULATION

Test	Oxidant-fuel ratio, O/F	Total pressure in nozzle, P_c, psia	Oxygen-injection differential pressure, psi	Hydrogen-injection differential pressure, ΔP, psi	Oxygen weight flow, $\dot{W}_{O_2}$, lb mass/sec	Hydrogen weight flow, $\dot{W}_{H_2}$, lb mass/sec	Chugging frequency, f, Hz	Peak-to-peak amplitude, psi
98	4.97	286	17	65	14.31	2.88	90	43
99	4.43	258	13	21	13.42	3.03	80	15
100	2.32	319	26	66	12.82	5.53	60 to 90	40
101	4.49	654	60	175	28.17	6.27	100	25
129	4.17	837	109	165	35.45	8.50	180	165

TABLE V. - FINE-ELEMENT INSTABILITY TABULATION

Test	Total pressure, in nozzle, psia	Oxidant-fuel ratio, O/F	Hydrogen injector temperature, ^{o}R	Screech frequency, f, Hz	Peak-to-peak amplitude, psi	Longitudinal mode
217	554	7.47	90	1000	45	2
219	767	5.73	68	750	30	1

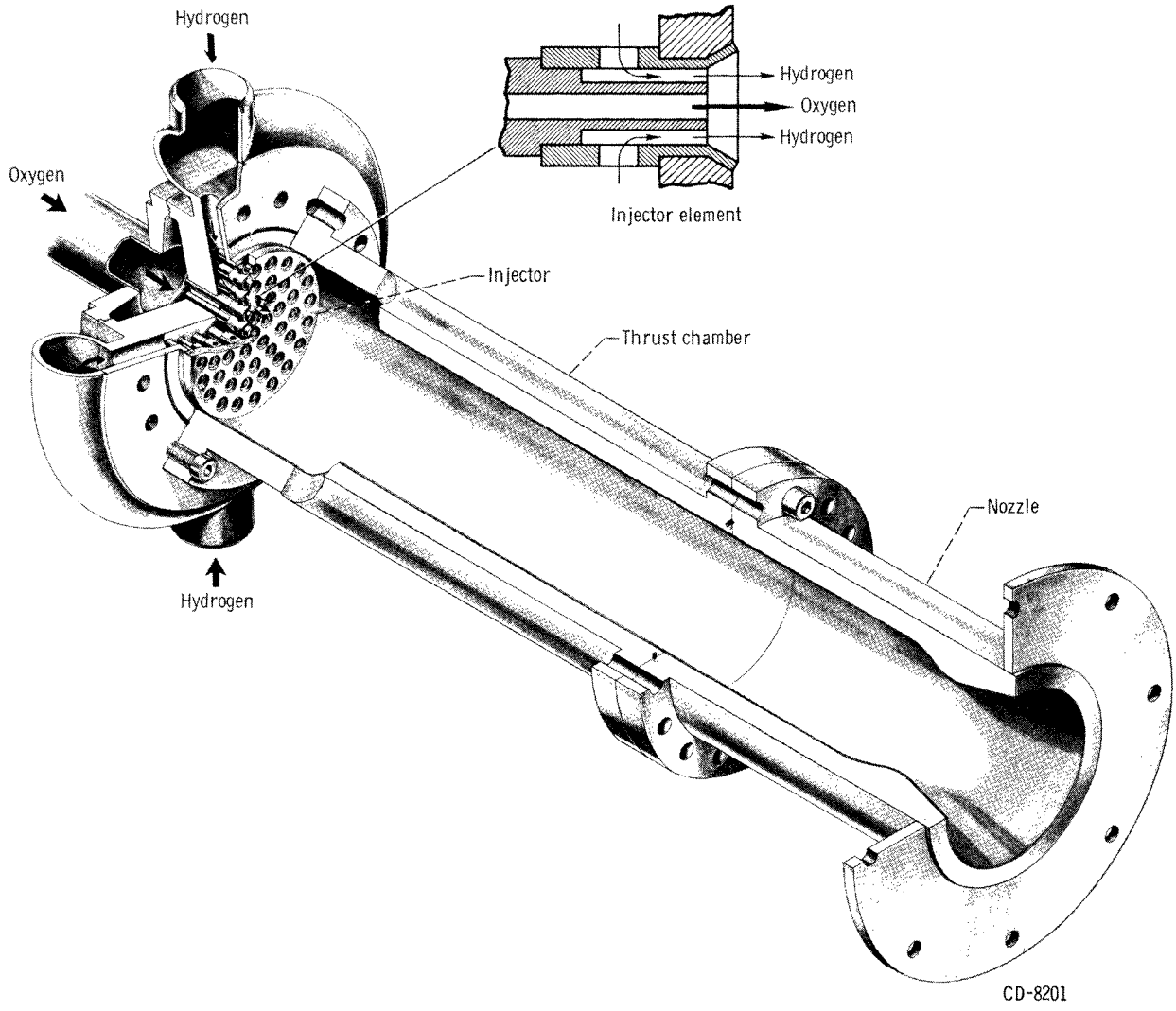

Figure 1. - Subscale engine.

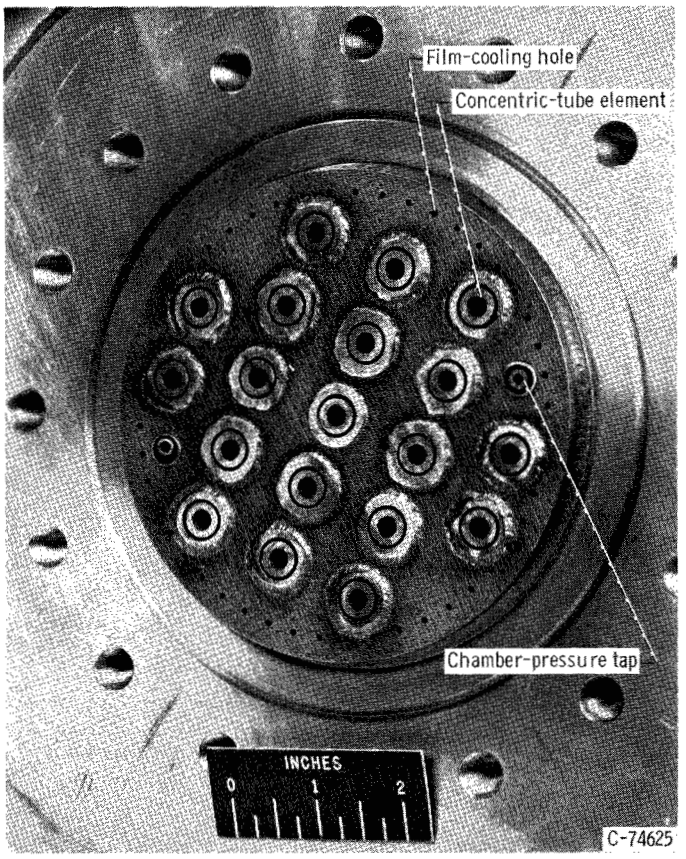

Figure 2. - Coarse-element injector. Thrust per element, 1267 pounds.

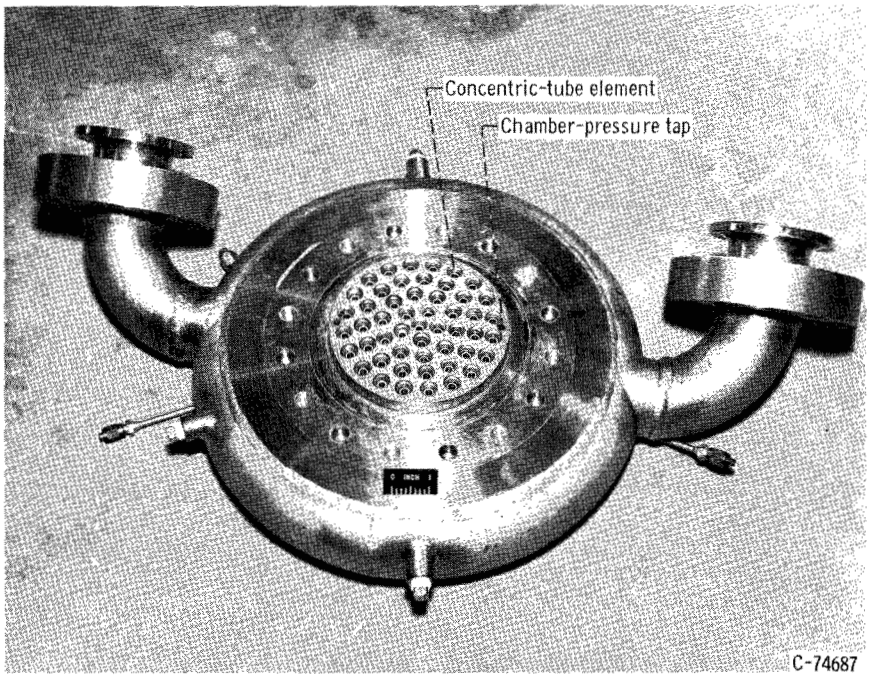

Figure 3. - Fine-element injector. Thrust per element, 462 pounds.

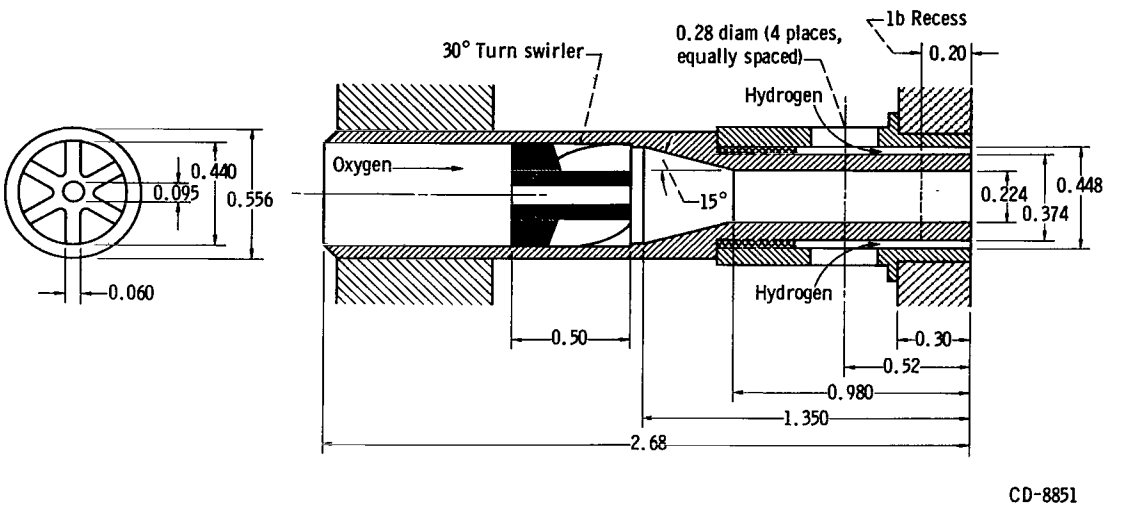

Figure 4. - Coarse elements. Configurations 1a and 1b are identical except for the oxygen-tube recess shown for 1b. (All linear dimensions are in inches.)

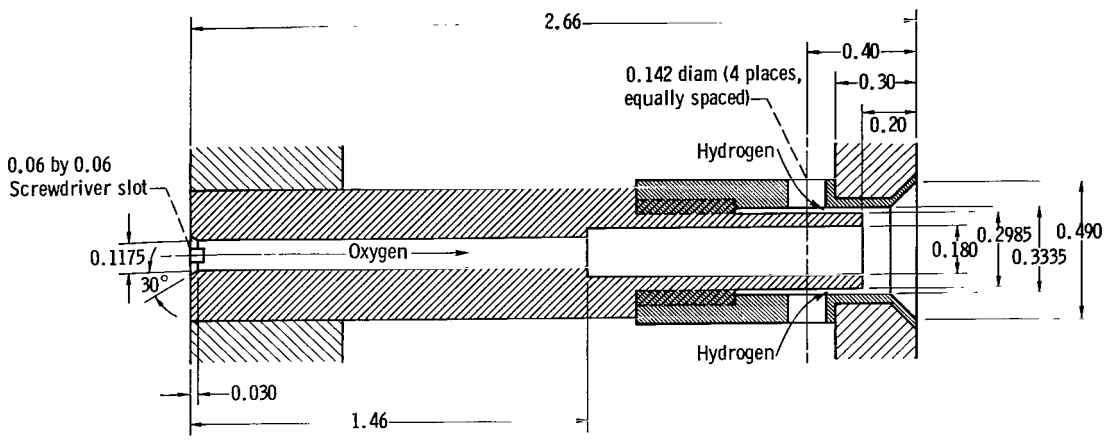

(a) Configuration 2a.

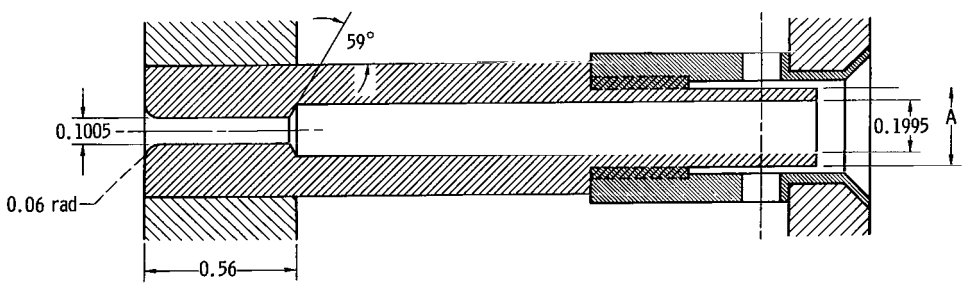

(b) Configurations 2b and 2c. Diameter A is 0.2985 inch for 2b and 0.290 inch for 2c.

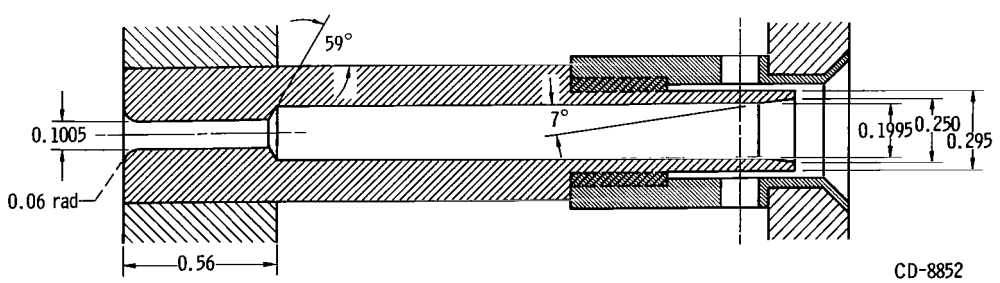

(c) Configuration 2d.

Figure 5. - Fine elements. (All linear dimensions are in inches.)

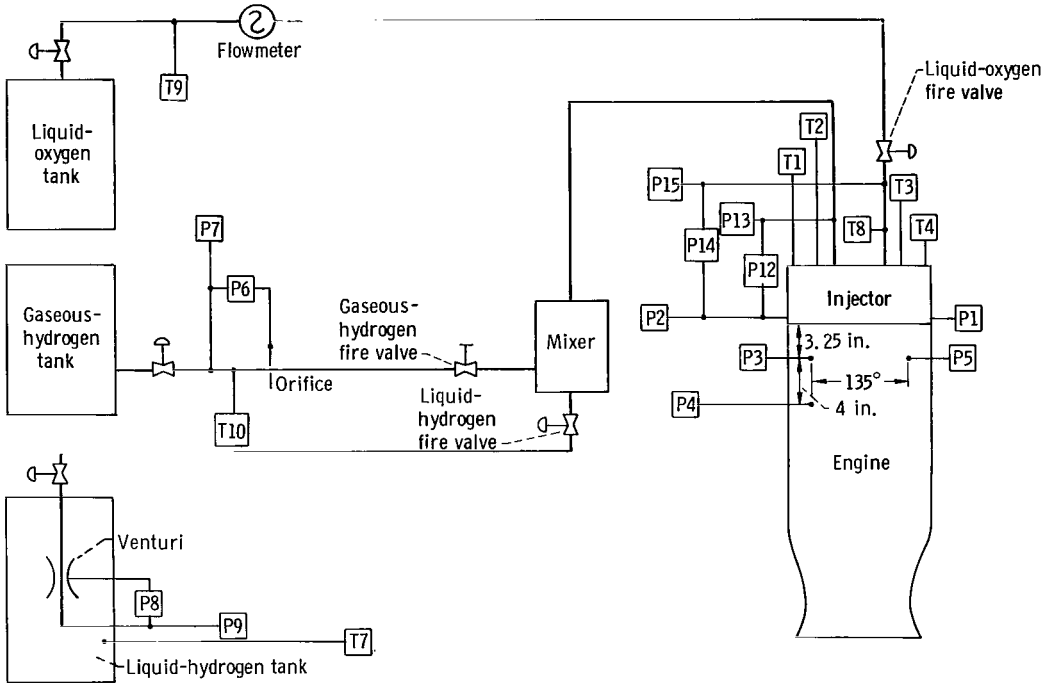

P1	Static chamber pressure (injector face), four-arm strain-gage transducer 1
P2	Static chamber pressure (injector face), four-arm strain-gage transducer 2
P3	Dynamic chamber pressure, water-cooled quartz pressure transducer 3
P4	Dynamic chamber pressure, water-cooled quartz pressure transducer 4
P5	Dynamic chamber pressure, water-cooled quartz pressure transducer 5
P6	Gaseous-hydrogen orifice differential pressure, four-arm strain-gage transducer
P7	Gaseous-hydrogen orifice pressure, four-arm strain-gage transducer
P8	Liquid-hydrogen venturi differential pressure, four-arm strain-gage transducer
P9	Liquid-hydrogen venturi pressure, four-arm strain-gage transducer
P12	Hydrogen-injection differential pressure, four-arm strain-gage transducer
P13	Hydrogen-injector pressure, four-arm strain-gage transducer
P14	Oxygen-injection differential pressure, four-arm strain-gage transducer
P15	Oxygen-injector pressure, four-arm strain-gage transducer
T1	Hydrogen-injector temperature, carbon-resistor-sensor probe 1
T2	Hydrogen-injector temperature, carbon-resistor-sensor probe 2
T3	Hydrogen-injector temperature, carbon-resistor-sensor probe 3
T4	Hydrogen-injector temperature, carbon-resistor-sensor probe 4
T7	Liquid-hydrogen venturi temperature, platinum resistor sensor
T8	Oxygen-injector temperature, copper-constantan thermocouple
T9	Oxygen flowmeter temperature, platinum resistor sensor
T10	Gaseous-hydrogen orifice temperature, iron-constantan thermocouple

Figure 6. - Instrumentation diagram.

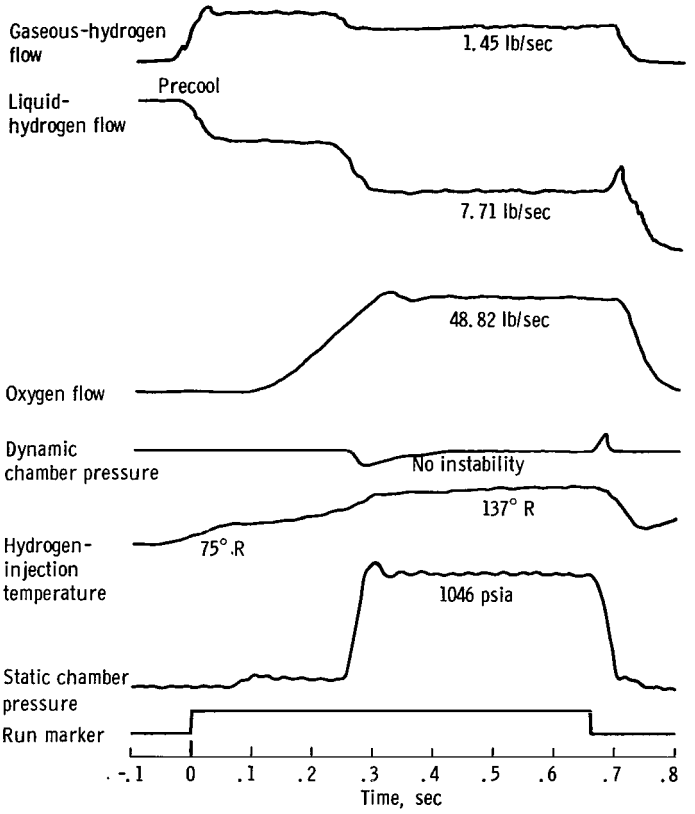

Figure 7. - Typical oscillograph record.

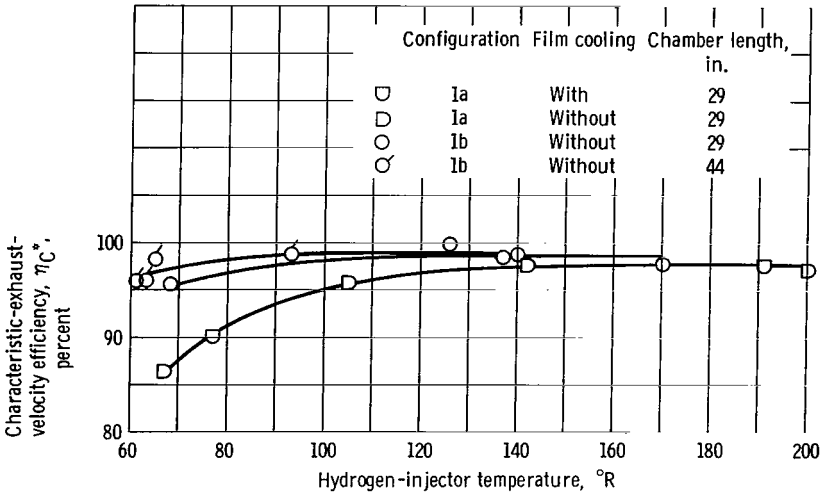

Figure 8. - Coarse-injector performance. Chamber pressure at injector face, 1040±100 psia; oxidant-fuel ratio, 5.5±1.0.

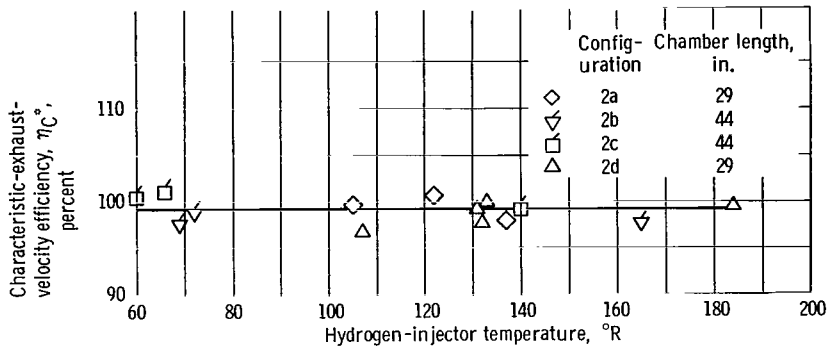

Figure 9. - Fine-injector performance. Chamber pressure at injector face, 1040±100 psia; oxidant-fuel ratio, 5.5±1.0; no film cooling.

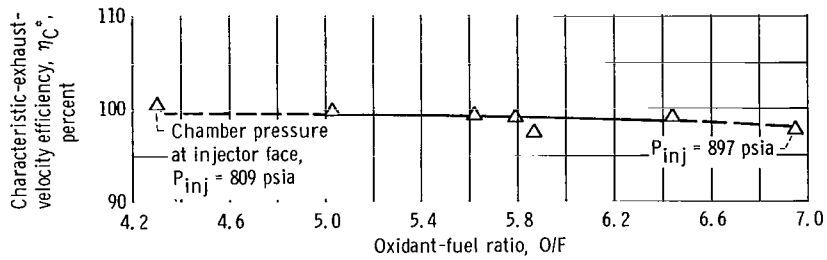

Figure 10. - Configuration 2d performance. Nominal chamber pressure at injector face, 1040 psia; nominal hydrogen-injector temperature, 140° R.

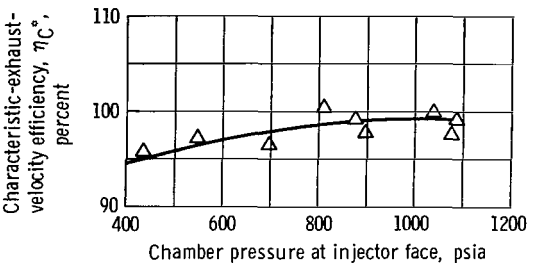

Figure 11. - Chamber pressure effect on performance of configuration 2d. Nominal hydrogen-injector temperature, 140° R.

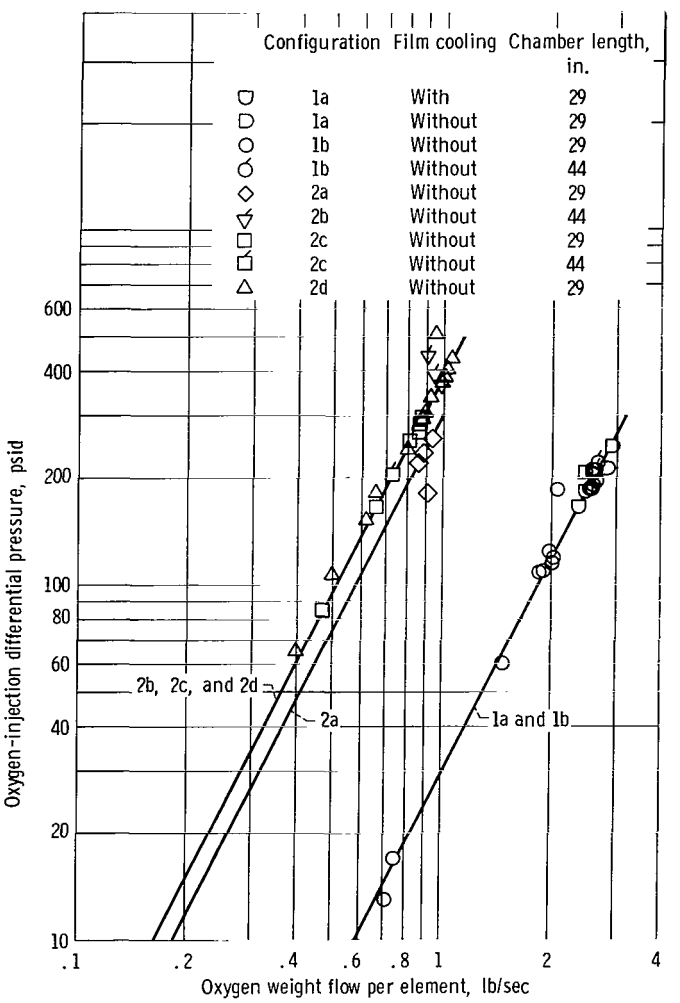

Figure 12. - Oxygen-injection flow characteristics. Slope of lines equals 2.

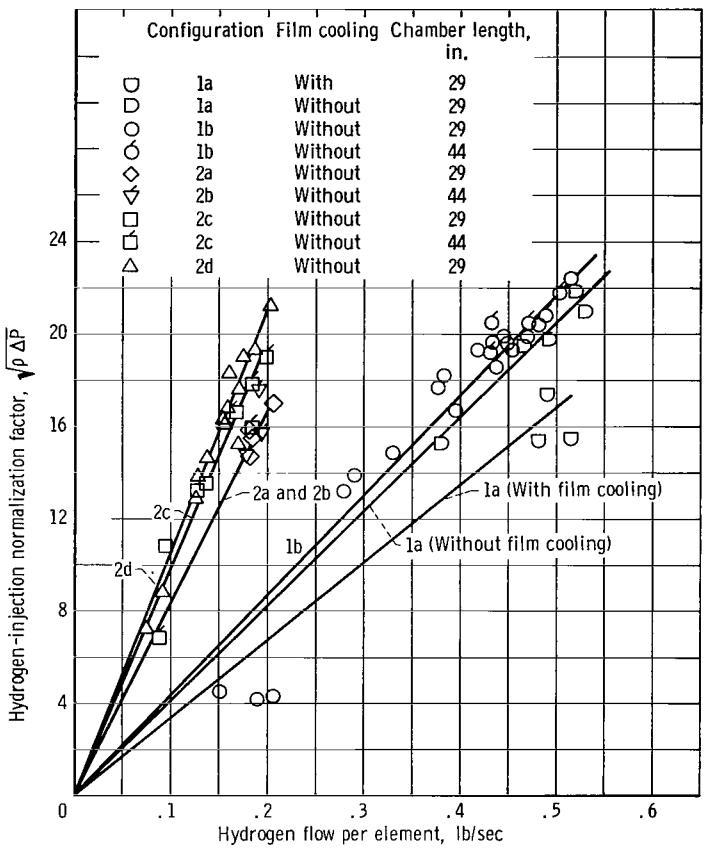

Figure 13. - Hydrogen-injection flow characteristics.

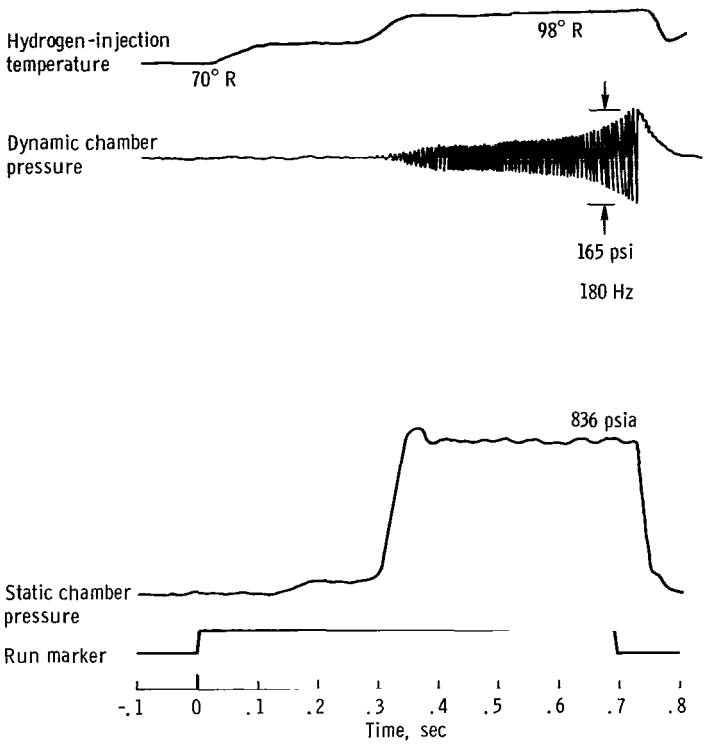

Figure 14. - Typical chugging run.

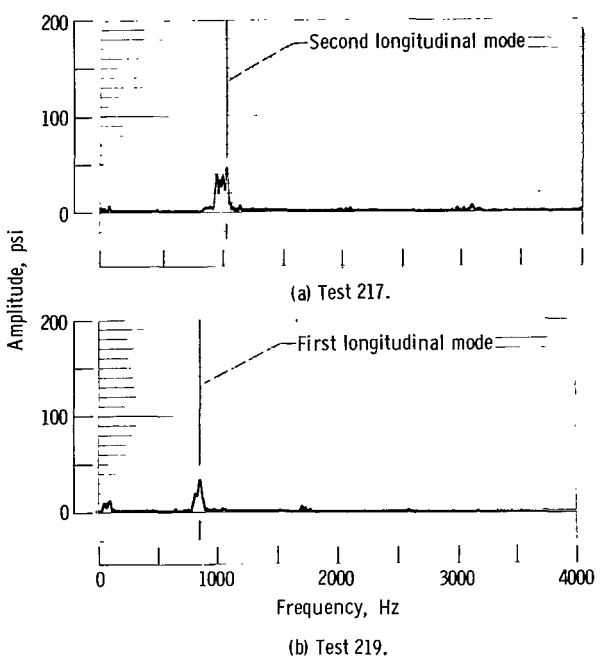

Figure 15. - Power spectral densities of screech occurrences.

"The aeronautical and space activities of the United States shall be conducted so as to contribute . . . to the expansion of human knowledge of phenomena in the atmosphere and space. The Administration shall provide for the widest practicable and appropriate dissemination of information concerning its activities and the results thereof."

—NATIONAL AERONAUTICS AND SPACE ACT OF 1958

NASA SCIENTIFIC AND TECHNICAL PUBLICATIONS

TECHNICAL REPORTS: Scientific and technical information considered important, complete, and a lasting contribution to existing knowledge.

TECHNICAL NOTES: Information less broad in scope but nevertheless of importance as a contribution to existing knowledge.

TECHNICAL MEMORANDUMS: Information receiving limited distribution because of preliminary data, security classification, or other reasons.

CONTRACTOR REPORTS: Scientific and technical information generated under a NASA contract or grant and considered an important contribution to existing knowledge.

TECHNICAL TRANSLATIONS: Information published in a foreign language considered to merit NASA distribution in English.

SPECIAL PUBLICATIONS: Information derived from or of value to NASA activities. Publications include conference proceedings, monographs, data compilations, handbooks, sourcebooks, and special bibliographies.

TECHNOLOGY UTILIZATION PUBLICATIONS: Information on technology used by NASA that may be of particular interest in commercial and other non-aerospace applications. Publications include Tech Briefs, Technology Utilization Reports and Notes, and Technology Surveys.

Details on the availability of these publications may be obtained from:

SCIENTIFIC AND TECHNICAL INFORMATION DIVISION

NATIONAL AERONAUTICS AND SPACE ADMINISTRATION

Washington, D.C. 20546